Application of Functional Modification of Iron-Based Materials in Advanced Oxidation Processes (AOPs)

Mengting Liu [1,†], Zhenzhen Zhao [1,†], Chiquan He [1,*], Feifei Wang [1], Xiaoyan Liu [1], Xueping Chen [1], Jialin Liu [2,3] and Daoyuan Wang [1,*]

1   Department of Environmental Science and Engineering, Shanghai University, Shanghai 200444, China; mtinglshe@163.com (M.L.); zzz0828@shu.edu.cn (Z.Z.); feifeiwang@shu.edu.cn (F.W.); lxy999@shu.edu.cn (X.L.); xpchen@shu.edu.cn (X.C.)
2   Shanghai Academy of Landscape Architecture Science and Planning, Shanghai 200232, China; jialinliu@seas.harvard.edu
3   Laboratory of Urban Design and Science, New York University Shanghai, Shanghai 200122, China
*   Correspondence: cqhe@shu.edu.cn (C.H.); dywang20@shu.edu.cn (D.W.); Tel.: +86-13816241151 (D.W.)
†   These authors contributed equally to this work.

Abstract: Advanced oxidation processes (AOPs) have become a favored approach in wastewater treatment due to the high efficiency and diverse catalyzed ways. Iron-based materials were the commonly used catalyst due to their environmental friendliness and sustainability in the environment. We collected the published papers relative to the application of the modified iron-based materials in AOPs between 1999 and 2020 to comprehensively understand the related mechanism of modified materials to improve the catalytic performance of iron-based materials in AOPs. Related data of iron-based materials, modification types, target pollutants, final removal efficiencies, and rate constants were extracted to reveal the critical process of improving the catalytic efficiency of iron-based materials in AOPs. Our results indicated that the modified materials through various mechanisms to enhance the catalytic performance of iron-based materials. The principal aim of iron-based materials modification in AOPs is to increase the content of available Fe^{2+} and enhance the stability of Fe^{2+} in the system. The available Fe^{2+} is elevated by the following mechanisms: (1) modified materials accelerate the electron transfer to promote the Fe^{3+}/Fe^{2+} reaction cycle in the system; (2) modified materials form chelates with iron ions and bond with iron ions to avoid Fe^{3+} precipitation. We further analyzed the effect of different modifying materials in improving these two mechanisms. Combining the advantages of different modified materials to develop iron-based materials with composite modification methods can enhance the catalytic performance of iron-based materials in AOPs for further application in wastewater treatment.

Keywords: advanced oxidation processes (AOPs); iron-based materials; modification; organic pollutant

1. Introduction

The treatment of refractory organic pollutants in water has been one of the most critical environmental issues during the past few decades [1–3]. Traditional chemical, physical, and biological methods treatment methods have been applied to treat refractory organic pollutants [4,5]. The advanced oxidation processes (AOPs) and functional iron-based materials have gradually attracted attention due to their high efficiency and policy development in the sewage treatment industry [6–8]. The most widely used AOPs processes include photochemical degradation processes (UV/O_3, UV/H_2O_2), photocatalysis (TiO_2/UV, photo-Fenton reactives), and chemical oxidation processes (O_3, O_3/H_2O_2, H_2O_2/Fe^{2+}) (Table 1) [9]. Meanwhile, alternative persulfate-AOPs utilizing peroxymonosulfate (PMS) or peroxydisulfate (PDS) instead of H_2O_2 have emerged and been researched in wastewater treatment [10].

Table 1. The types of AOPs processes in wastewater treatment.

Types of AOPs System	Types of AOPs Processes				
	Process of AOPs Based on $OH^{\cdot}$			Process of AOPs Based on SO_4^{-}	
	Photochemical	Photocatalysis	Chemical Oxidation Processes	Persulfate-AOPs	
	UV/O_3, UV/H_2O_2	TiO_2/UV, Photo-Fenton Reactives	O_3, $O_3/$ H_2O_2, H_2O_2/Fe^{2+}	Peroxymonosulfate (PMS)-AOPs	Peroxydisulfate (PDS)-AOPs
Oxidation process	$AOPs \rightarrow OH^{\cdot} \xrightarrow{pollutant} CO_2 + H_2O$			$AOPs \rightarrow SO_4^{-} \xrightarrow{pollutant} CO_2 + H_2O$	
Oxidation properties	$E_0 \left(OH^{\cdot}/OH^{-} \right) = +1.90 - +2.70 \, V_{NHE}$			$E_0 \left(SO_4^{-}/SO_4^{2-} \right) = +2.60 - +3.10 \, V_{NHE}$	

Nanomaterials have properties of high surface area and high catalytic activity, which have been increasingly employed in AOPs [11,12]. Currently, the nanomaterials used in AOPs include carbon-based nanomaterials, metal-based nanomaterials, zeolite, TiO_2, etc. [13]. Iron-based nanomaterials, as a kind of metal-based nanomaterials, have also been widely used in AOPs due to their environmentally friendly properties [14,15]. However, these materials also have limited mass transfer and poor stability [11]. Homogeneous AOPs based on Fe^{2+}, such as homogeneous Fenton systems or homogeneous persulfate (PS)/peroxymonosulfate (PMS) systems, have been accepted in practice due to their advantages, such as low cost, non-toxicity, and widely available [4,16,17]. The reactive oxidation substance (ROS) in AOPs, including hydroxyl radicals ($OH^{\cdot}$), sulfate radicals (SO_4^{-}), superoxide radicals (O_2^{-}), and singlet oxygen ($^1O_2$), ideally can induce the complete degradation of many pollutants [2,18]. However, homogeneous AOPs based on Fe^{2+} should be operated in highly restrictive conditions, such as low pH and high Fe^{2+} concentrations [19–21]. Meanwhile, the properties of easy agglomeration of iron-based materials also limit its application in the environment. Therefore, previous studies prioritized modifying iron-based materials to avoid those obstacles [8,22,23].

Iron-based materials are widely distributed in enormous quantities and can be environmentally friendly [24–26]. The functional modification of iron-based materials with environmentally friendly materials can improve the performance of iron-based materials and expand the sustainability of their applications in the natural environment [27,28]. We collected the literature about applying iron-based materials modification in AOPs from the Web of Science database. The application of various iron-based materials in AOPs was systematically analyzed, and the related factors affecting the catalytic performance of iron-based materials in AOPs were also analyzed. Finally, the related mechanisms of the modified materials that enhanced the catalytic performance of iron-based materials that were detailed were also analyzed.

2. Data Sources and Search Strategy

Published papers from 1999 to 2020 were systematically searched in databases such as the Web of Science using keywords [29] (Table S1), and 2028 articles were selected (Figure 1). After reading based on the title and abstract of the literature, the repeated books and conference literature were removed. In addition, relevant documents unrelated to iron-based materials and the use of adsorption to remove organic pollutants were also been removed. The number of documents selected in this process and finally entered into the evaluation stage was n = 467. Based on the second-stage literature screening, the screening scope was further narrowed by reading the complete text. The literature that was not related to advanced oxidation, iron-based materials and organic pollutants were eliminated. The number of documents selected in this process and finally entered into the evaluation stage is n = 100. In this stage, data including publication year, author, journal, materials used, target pollutant type, advanced oxidation type, reaction time, removal rate,

kinetic constant, and primary reactive oxidation substance (ROS) included in the screening literature were also extracted. Meanwhile, relevant impact factors such as temperature, pH, catalyst dosage, target pollutant concentration, oxidant dosage, and other data were also extracted [30]. All the relevant literature and extracted data are shown in the Excel table in the Supplementary Excel File S1.
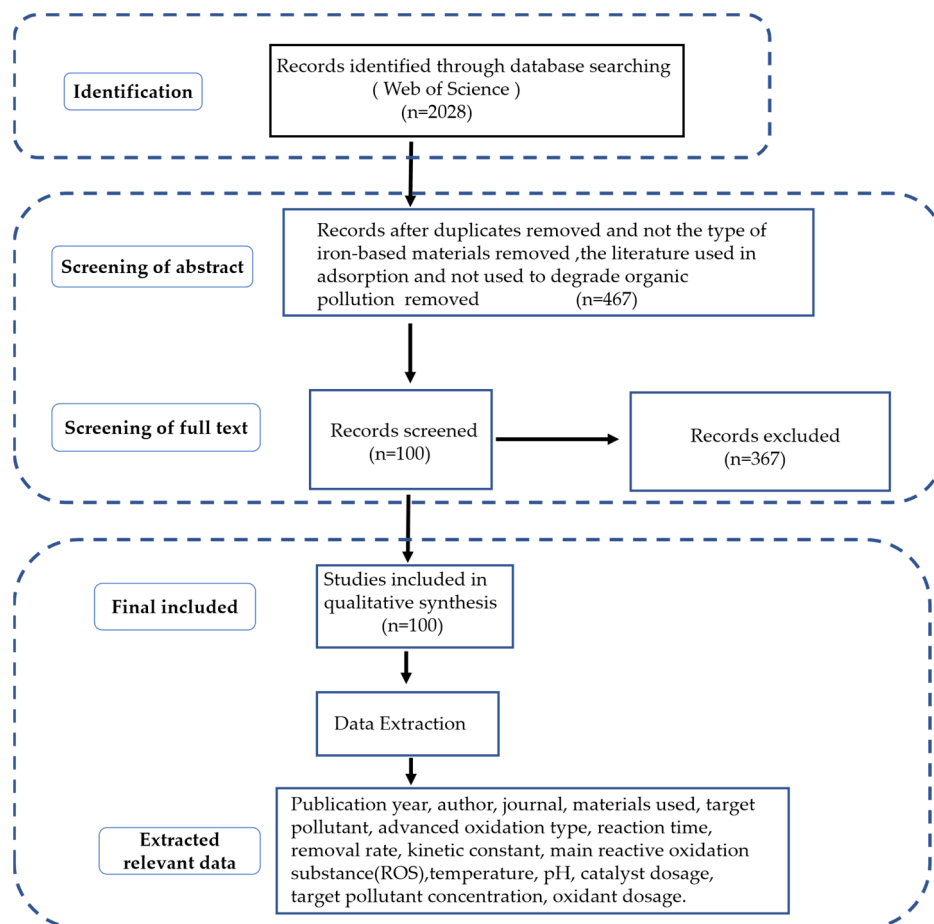
Figure 1. The flowchart of the search and selection of published papers based on the Web of Science database by using keywords.

As shown in Figure S1, documents obtained in the third stage of the document search were categorized according to the different types of organic pollutants, oxidation type, and iron-based materials. The primary pollutants treated by AOPs are medicines, dyes, endocrine disruptors, chlorinated hydrocarbons, and phenols (Figure S1a). The Fenton-based AOPs and PS/PMS-based AOPs have a preferential trend in removing organic compounds in water (Figure S1b). The primary iron-based materials currently used are zero-valent iron (ZVI), nano zero-valent iron (n-ZVI), Fe_2O_3, Fe_3O_4, FeOOH, FeO, Fe^{3+}, iron-based metal-organic framework (Fe-MOFs), metal ferrite (MFe_2O_4, M=Fe Co, Ni, Mn, Cu, Zn) (Figure S1c). Based on the published literature collected in the database, the primary modified materials are shown in Table S2.

3. Iron-Based Materials in AOPs: Systematic Classification and Mechanism Analysis

Iron-based materials vary in size, active sites, organic molecular transport channels, and iron ions valence [31–33]. The n-ZVI, as a source of non-photochemical ROS, has a higher specific surface area, particle size ratio, and more active sites than ZVI and Fe_2O_3. The n-ZVI facilitates electron transfer at its surface due to its advantage in active sites, resulting in higher reactivity in AOPs [2,34]. As a metal hydroxide, FeOOH widely exists in nature and is considered a semiconductor. Meanwhile, it was photoactive under solar

radiation due to its narrow bandgap of 2.0–2.3 eV absorbed 200–800 nm sunlight [35]. The photocatalytic activity and the generation of Fe^{2+} on the goethite surface make it an effective catalyst for PS/PMS or H_2O_2 [1,8]. The iron-based metal–organic framework (Fe-MOFs) has the characteristics of large surface area, large nano-scale cavities, open channels, and uniform distribution of metal centers [36–38]. Its open channels and sufficient nano-scale cavities are conducive to the diffusion of molecules, which provides more available active sites, which can be obtained by reactants [38]. Coordinated unsaturated metal sites generated in the activation process facilitated the H_2O_2 (Lewis base) adsorption due to the Lewis acidity of the metal cations [39]. Metal iron oxides such as spinel ferrite (MFe_2O_4, M=Ni, Cu, Zn, Co et al.) have received more attention in catalytic applications due to their magnetic recycling ability, stable crystal structure, high-density oxygen vacancies, and surface hydroxyl groups [17,40]. Liu et al. found that $CuFe_2O_4$ has more significant advantages in catalytic activity due to the more oxygen vacancies and surface hydroxyl groups than Fe_2O_3 [41].

Iron-based materials as catalysts to replace Fe^{2+} in the homogeneous AOPs, the content of available Fe^{2+} affects iron-based materials' catalytic performance [26]. It is worth noting that the primary iron element state of Fe^0 (ZVI and n-ZVI) is Fe^{2+} (Equations (1)–(3)) [34]. However, the materials such as Fe-MOFs, Fe_3O_4, Fe_2O_3, MFe_2O_4 (M=Ni, Cu, Zn, Co et al.), and FeOOH, containing the Fe^{3+} as their predominant iron element state [33,42,43]. Fe^{3+} as an electron acceptor cannot directly activate the oxidant, and the interaction with the oxidant led to the generation of weaker free radicals in AOPs. It is necessary to reduce Fe^{3+} to Fe^{2+} before reacting with oxidants to generate ROS, which is crucial in determining the reaction rate in AOPs. For example, Zhang et al. used Fe^{2+} and Fe^{3+} to activate H_2O_2 (Equations (4) and (5)). The rate constant of the k value when Fe^{3+} and Fe^{2+} are used as the H_2O_2 activator was 0.02 M^{-1} s^{-1} and 76 M^{-1} s^{-1}, respectively. There are three orders of magnitude differences in the rate constant of degradation target pollutants [39]. Chen et al. used Fe^{2+}/Fe^{3+} to activate PMS (HSO_5^-) (Equations (6) and (7)) and found that Fe^{2+} activation produced the main SO_4^{-}, while Fe^{3+} activated PMS to generate less oxidative free radical of SO_5^{-} [43]. Therefore, the Fe^{2+} content is a crucial factor for the degradation of target pollutants in AOPs [39,44].

$$Fe^0 \rightarrow Fe^{2+} + 2e^- \tag{1}$$

$$2Fe^0 + O_2 + 2H_2O \rightarrow 2Fe^{2+} + 4OH^- \tag{2}$$

$$Fe^0 + O_2 + 2H^+ \rightarrow Fe^{2+} + H_2O_2 \tag{3}$$

$$Fe^{2+} + H_2O_2 \rightarrow Fe^{3+} + OH^{\cdot} + OH^- \tag{4}$$

$$Fe^{3+} + H_2O_2 \rightarrow Fe^{2+} + HO_2 + H^+ \tag{5}$$

$$Fe^{2+} + HSO_5^- \rightarrow SO_4^{-} + Fe^{3+} + OH^- \tag{6}$$

$$Fe^{3+} + HSO_5^- \rightarrow Fe^{2+} + SO_5^{-} + H^+ \tag{7}$$
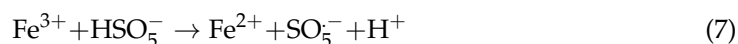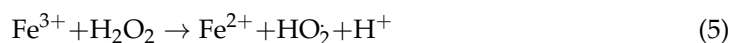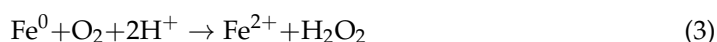
4. Mechanism of Modified Materials to Raise the Content of Fe^{2+} of Iron-Based Materials in AOPs

4.1. Modified Materials Accelerate the Electron Transfer in AOPs

4.1.1. Electron-Rich Functional Groups in Modified Materials Facilitate Electron Transport

Electron transfer during the interaction between iron-based materials and oxidants can increase the Fe^{2+} content of iron-based materials in AOPs [26]. In modifying iron-based materials, many modified materials have large functional groups, such as hydroxyl groups (-OH), ketone groups (-C=O), carboxyl groups (-COOH), etc. [45–47]. These oxygen-containing functional groups are electron-rich and act as electron donors to facilitate electron transfer from catalyst to oxidant in AOPs. Activated carbon, biochar, graphene, carbon nanotubes, as supporting materials in modifying iron-based materials, have large oxygen-containing functional groups such as hydroxyl groups (-OH), ketone groups (-C=O),

carboxyl groups (-COOH), etc. [48]. Guo et al. used carbon spheres to modify Fe_3O_4. The Lewis basic groups, such as plenteous ketone groups (-C=O), on the surface of the magnetic carbon shell combined with PMS molecules and promoted the electron transfer process in AOPs. The electrons transferred from the catalyst to the PMS generated more ROS, which can contribute to target pollutant degradation [49]. Luo et al. have found that biochar that transferred electrons to n-ZVI promoted the formation of the active substance Fe^{2+} in the Fenton-like AOPs [1,50]. Yao et al. found that the functional groups on the biochar surface had an activating effect, which acted as an electron shuttle in the PS-based AOPs to mediate the transfer of conductive electrons and activated the oxidant to generate a strong oxidizing active SO_4^- (Equations (8) and (9)) [21].

$$SBC_{surface}-OOH + S_2O_8^{2-} \rightarrow SBC_{surface}-OO^{\cdot} + SO_4^- + HSO_4^- \tag{8}$$

$$SBC_{surface}-OH + S_2O_8^{2-} \rightarrow SBC_{surface}-O^{\cdot} + SO_4^- + HSO_4^- \tag{9}$$
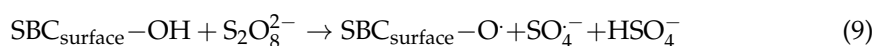
Clay minerals are dual-functional materials with adsorption and catalytic oxidation capabilities [51–53]. Clay minerals, including montmorillonite and natural sepiolite, have abundant -OH as supporting materials in modifying iron-based materials [52,54]. Niu et al. have shown that montmorillonite was rich in -OH and was always negatively charged in a wide pH range (2–11), which facilitated H_2O_2 adsorption and was further conducive to the rate-controlled decomposition of H_2O_2 in the reaction [54]. The presence of the opposing surface also formed a proton-rich layer on the surface and improved the selectivity of H_2O_2 to decompose $OH^{\cdot}$. Liu et al. reported that sepiolite as $CuFe_2O_4$-supporting materials played an essential role in dispersing the active phase and promoted oxygen migration from the active site to the oxygen vacancy, which was very important in the electron transfer in AOPs and light-based AOPs. The -OH on the surface and other Lewis acid sites could promote O_3 decomposition to generate more $OH^{\cdot}$ [41].

4.1.2. Redox Pairs in the Bimetallic System Facilitates Electron Transfer

The redox pairs in the bimetallic system formed by the modification of iron-based materials plays a crucial role in electron transfer. On one hand, single metal as the second metal such as Ni, Ag, Cu, Co, and Al was deposed on the surface of the iron-based materials to form a bimetallic system [55–57]. Notably, the metal additives may prevent or delay the formation of an iron oxide shell, which maintains the catalytic ability of ZVI/n-ZVI for a longer time. In addition, metal additives in bimetallic systems can serve as electron donors, promoting electron transfer in AOPs [58,59]. For example, Liu et al. found that zero-valent aluminum (ZVAl) could provide a greater thermodynamic driving force for electron transfer on the facile transfer of electrons to O_2, which enhanced the catalytic ability of the nanoparticles [60]. Meanwhile, the redox pair present in the bimetal system can promote the circulation of Fe^{3+}/Fe^{2+}, increasing the content of effective Fe^{2+} to enhance the performance of AOPs [4,61]. Xu et al. found that Cu-doped FeOOH composites promoted electron transfer between copper ions and iron ions. $Cu+/Cu^{2+}$ could promote the cycle of Fe^{3+}/Fe^{2+} in the system, which produced more ROS to degrade pollutants (Equations (10) and (11)) [1]. Zhang et al. introduced cobalt into iron to form a bimetallic catalyst and improved interface electron transfer due to dual-redox pairs (Fe^{3+}/Fe^{2+} and Co^{2+}/Co^{3+}) in the system [6,62].

$$Fe^{2+} + S_2O_8^{2-} \rightarrow Fe^{3+} + SO_4^{2-} + SO_4^- \tag{10}$$

$$Cu^+ + Fe^{3+} \rightarrow Cu^{2+} + Fe^{2+} \tag{11}$$

On the other hand, the redox pairs in the mixed metal catalyst were formed by supporting metal oxides, as the modification of iron-based materials can promote the electron transfer and improve the catalytic activity of the oxidant in AOPs. Lu et al. used MnO_2-loaded beta-FeOOH catalyst as a catalyst for PMS, the redox pairs of Mn^{4+}/Mn^{3+}

and Fe^{3+}/Fe^{2+} could more effectively catalyze PMS to generate more ROS in AOPs (Equations (12)–(16)) [63,64].

$$-Mn^{4+}+HSO_5^- \rightarrow -Mn^{3+}+SO_5^- +H^+ \tag{12}$$

$$-Mn^{3+}+H_2O \rightarrow -MnOH^{2+}+H^+ \tag{13}$$

$$-Fe^{3+}+HSO_5^- \rightarrow -Fe^{2+}+SO_5^- +H^+ \tag{14}$$

$$-Fe^{2+}+H_2O \rightarrow -FeOH^+ +H^+ \tag{15}$$

$$-Mn^{4+}+-Fe^{2+} \rightarrow -Mn^{3+}+Fe^{3+} \tag{16}$$
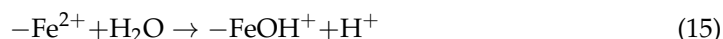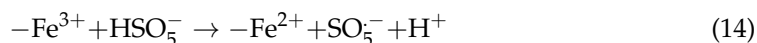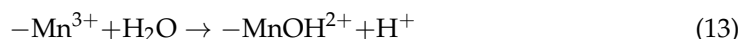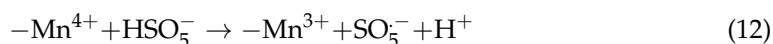
4.1.3. The FeS Layer Formed during Sulfide Modification of Iron-Based Materials Promotes Electron Transport

The solid Fe-S bond formed in the FeS layer on the surface of iron-based materials played an essential role in improving the catalytic performance of composite materials in AOPs. As shown in Figure 2, the sulfide-modified iron-based material with a core-shell structure formed an outer layer of FeS with unique physical and chemical properties [65–67]. The FeS layer had a protective effect for iron-based materials, acted as an electron shuttle to transfer electrons, and promoted the corrosion of n-ZVI to release effective Fe^{2+} [2]. The direct reaction of n-ZVI with oxygen was greatly restricted due to the more stable Fe-S bond in the FeS layer [62,68]. Meanwhile, Fe-S clusters, as an electric "wire", promoted the direct electron transfer of the Fe^0 nucleus to Fe^{3+} and promoted the cycle of Fe^{3+}/Fe^{2+}, so a large amount of effective state of Fe^{2+} was bound to the surface [62]. Therefore, the presence of the Fe-S layer significantly enhanced the yield of ROS in the system and played a significant role in the degradation of target pollutants [65].
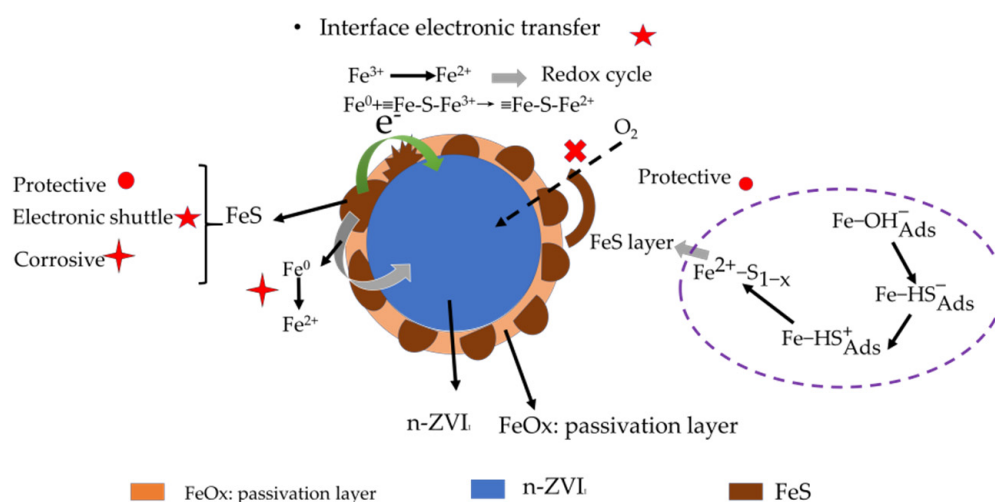
Figure 2. The mechanism of vulcanization modification of n-ZVI improves organic pollutants' removal efficiency in AOPs.

4.1.4. Quinone Structure Formed by Organic Quinones-Modified Iron-Based Materials as Electron Shuttle Mediators to Facilitate Electron Transfer

Organic quinones with the redox potential act as redox shuttles, which can accelerate electron transfer during the modification of iron-based materials. Xiang et al. modified Fe-MOFs with quinone, in which the quinone unit (Q) in 2-anthraquinone sulfonate (AQS) could be reduced to form semiquinone (SQ) or hydroquinone (HQ). The interaction effect of Fe^{3+} with SQ or HQ promoted the Fe^{3+}/Fe^{2+} cycling in the system (Equations (17)–(21) [33]. Biochar as a supporting material also contains a hydroquinone/quinone structure, which played an essential role in the functional modification of iron-based materials [4,47]. Wang et al. reported that the hydroquinone/quinone structure in biochar promoted the Fe^{2+}/Fe^{3+} cycling by acting as an electron donor [69–71]. Biochar hydroquinone (BCHQ) to quinone

(BCQ) during the interaction between biochar and iron-based materials increased the Fe^{2+} content and the ROS generation, which further improved the catalytic performance of iron-based materials in AOPs (Equations (22)–(24)).

$$Q + H_2O \rightarrow 2SQ + 2H^+ \tag{17}$$

$$Q + O_2^{\cdot -} \rightarrow SQ + O_2 \tag{18}$$

$$SQ + O_2^{\cdot -} \rightarrow HQ + O_2 \tag{19}$$

$$Fe^{3+} + SQ \rightarrow Fe^{2+} + Q + H^+ \tag{20}$$

$$Fe^{3+} + HQ \rightarrow Fe^{2+} + SQ + H^+ \tag{21}$$

$$BC \equiv Fe^{2+} \rightarrow Fe^{2+} \, (\text{dissolution}) \tag{22}$$

$$Fe^{2+} + H_2O_2 \rightarrow Fe^{3+} + OH^- + OH^{\cdot} \tag{23}$$

$$Fe^{3+} + BCHQ \rightarrow Fe^{2+} + BCQ \tag{24}$$
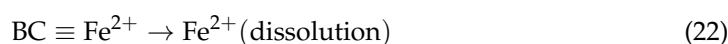
4.1.5. The Unique Hybrid Structure Formed by Non-Metal Element-Doped Carbon-Based Materials Promotes Electron Transfer

Carbon-based materials, e.g., activated carbon, graphene, carbon nanotubes, can be functionalized by doping non-metallic elements such as boron, nitrogen, sulfur [48,72,73]. The unique hybrid structure increased functional materials' catalytically active sites and conductivity [4,74,75]. Li, M et al. found that an appropriate sp^2/sp^3 hybrid structure effectively increased the electron density on the surface of graphitized carbon, transferred more electrons to the PMS molecule, and accelerated the oxidation process [76,77]. Liu et al. found that metal nanocrystals synergized with nitrogen-doped carbon to facilitate electron transfer to maintain Fe^{2+} regeneration. The sp^2 hybrid carbon network with many mobile electrons efficiently activated PMS to generate ROS to degrade target pollutants (Equation (25)) [6,78]. Xu et al. found that boron-doped activated carbon destroyed the electroneutrality of the original carbon material, resulting in the electron rearrangement of adjacent carbon atoms. At the same time, it was easier to form CO bonds on the carbon atoms adjacent to boron, which promoted the redox reactions in electron-rich centers [79]. Liu et al. found that sulfur-doped activated carbon formed the unique C-S-C bond. The unique C-S-C bond has electron-rich properties that promote electron transfer to the PMS [80].

$$C - \pi^- + HSO_5^- \rightarrow C - \pi + OH^- + SO_4^{\cdot -} \tag{25}$$
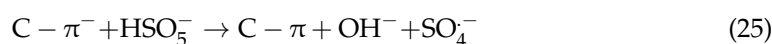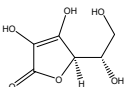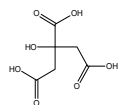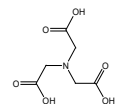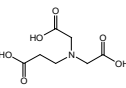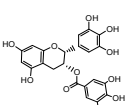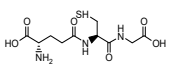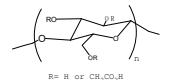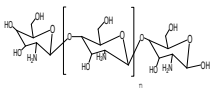
4.2. Modified Materials to form Iron Complex or Surface Bonding with Iron to Increase Fe^{2+}

4.2.1. Formation of Iron Ion-Chelates Using Chelating Agents as Stabilizers for Iron-Based Materials to Increase Fe^{2+}

The chelating agent can reduce the precipitation of iron ions in AOPs by forming iron chelate complexes with iron-based materials during using chelating agents as stabilizer materials to modify iron-based materials. The formation of iron chelates could further increase the Fe^{2+} content and produce more ROS in AOPs [81–83]. Ascorbic acid (VC), citrate (Cit), nitrilotriacetic acid (NTA), β-alaninediacetic acid (β-ADA), epigallocatechin gallate (EGCG), etc. can form iron chelates such as $VC \cdots Fe^{3+}$, $Fe^{3+} - Cit$, $Fe^{2+} - NTA$, $Fe^{2+} \cdots \beta - ADA$, $Fe^{3+} \cdots EGCG$ (Table 2), which can significantly improve the solubility of Fe^{2+} in AOPs [25,84]. Tan et al. found that $VC@Fe_3O_4$ composite material enhanced the removal efficiency of sulfadiazine from 40% to 57% compared with Fe_3O_4 alone, and the rate constant k value was increased from 0.01 min^{-1} to 0.072 min^{-1} [82]. The composite material formed by citrate and Fe_2O_3 elevated the removal efficiency of methylene blue from 20% to 96.1%, and the rate constant k value was increased from 0.002 min^{-1} to 0.0463 min^{-1} [25]. The composite material formed by NTA and Fe_2O_3 improved the removal efficiency of sulfamethazine from 20% to 96.1%, and the rate constant k value was increased from 0.007 min^{-1} to 0.1954 min^{-1} [81]. As shown in

Table 2, stabilizer materials also have many functional groups, such as C=O, -OH, C-O, -COO, -NH$_2$, -SH, -COOH [20,76,82]. These active groups could chelate iron ions and enhance the direct contact between the iron-based material and the oxidant or target pollutants [84]. Zhou et al. found that the glutathione (GSH) was anchored onto the surface of Fe$_3$O$_4$ nanoparticles via the thiol groups in modifying Fe$_3$O$_4$ particles, and the Fe^{2+} leached from the Fe$_3$O$_4$ attracted by the coated GSH can effectively react with the nearby H$_2$O$_2$ to generate OH$^.$ to achieve the high efficient pollutant removal [85]. Bio-friendly polymers also have an excellent chelating ability with iron ions. Wang et al. found that Fe$_3$O$_4$ @β-CD with particular structure of β-CD has higher catalytic ability than pure Fe$_3$O$_4$, and Fe^{2+}-β-CD-pollutant complexes allowed the production of OH$^.$ directly attacked pollutants and increased the solubility of organic pollutants [86]. Fe$_3$O$_4$ @β-CD composite material enhanced the removal efficiency of 4-chlorophenol from 78% to 100% compared with Fe$_3$O$_4$ alone, and the rate constant k value was increased from 0.0162 min^{-1} to 0.0373 min^{-1}. Nadejde et al. synthesized chitosan (CS) and Fe$_3$O$_4$ composite material (Fe$_3$O$_4$/CS) for high-efficiency catalytic degradation of bisphenol A. The Fe^{2+} or Fe^{3+} combined with the CS surface to the biopolymer, which acted as a ligand between the magnetic core and the external photoactive agent [87]. The composite material formed by CS and Fe$_3$O$_4$ strengthened the removal efficiency of bisphenol A from 30% to 98%, and the rate constant k value was increased from 0.0009 min^{-1} to 0.0031 min^{-1}. These chelating agents were environmentally friendly with low toxicity and high biodegradability [25,42,76].

Table 2. Summary of related properties and reactions of different types of stabilizer materials in AOPs.

Stabilizer Materials		Structure	Functional Groups	Reactions	Reference
Chelating agent	Ascorbic acid(VC)		-OH -C-O	$VC \cdots Fe^{3+} \rightarrow MDHA \cdots Fe^{2+} + H^+$ $Fe^{2+} + HSO_5^- \rightarrow SO_4^- + Fe^{3+} + OH^-$ $SO_4^- + H_2O \rightarrow OH \cdot + HSO_4^-$	[82]
	Citrate		-COOH -OH	$Fe^{3+} - Cit + hv \rightarrow Fe^{2+} + .OOC - C(OH)(CH_2COO)_2{}^{2-}$ $.OOC - C(OH)(CH_2COO)_2{}^{2-} \rightarrow .C(OH)(CH_2COO)_2{}^{2-} + CO_2$ $.C(OH)(CH_2COO)_2{}^{2-} + O_2 \rightarrow CO(CH_2COO)_2{}^{2-} + HO_2 \cdot$ $Fe^{2+} + HO_2 \cdot + H^+ \rightarrow Fe^{3+} + H_2O_2$ $Fe^{2+} + H_2O_2 \rightarrow Fe^{3+} + OH \cdot + OH^-$	[25]
	Nitrilotriacetic acid(NTA)		-COOH C=O -C-O-OH	$Fe^{2+} - NTA + H_2O_2 \rightarrow Fe^{3+} - NTA + OH \cdot + OH^-$ $Fe^{3+} - NTA + H_2O_2 \rightarrow Fe^{3+}OOH^{-1}NTA + H^+$ $Fe^{3+}OOH^{-1}NTA + H_2O_2 \rightarrow Fe^{2+}ONTA + HO_2 \cdot + H_2O$	[81]
	β-alanine diacetic acid(β-ADA)		-COOH -C-O -OH	$Fe^{2+} \cdots \beta - ADA + HSO_5^- \rightarrow Fe^{3+} \cdots \beta - ADA + SO_4^- + OH^-$ $SO_4^- + H_2O \rightarrow SO_4^{2-} + OH \cdot + H^+$ $Fe^{3+} \cdots \beta - ADA + HSO_5^- \rightarrow Fe^{2+} \cdots \beta - ADA + SO_5^- + H^+$	[83]
	Epigallocatechin gallate(EGCG)		-OH	$Fe^{3+} \cdots EGCG + HSO_5^- \rightarrow Fe^{2+} - .OOSO_3^- + EGCG^+$ $Fe^{2+} + HSO_5^- \rightarrow Fe^{3+} + SO_4^- + OH^-$ $Fe^{2+} - OH^- + HSO_5^- \rightarrow Fe^{2+} - (HO)OSO_3^- + OH^-$ $Fe^{2+} - (HO)OSO_3^- \rightarrow Fe^{3+} - OH^- + SO_4^-$ $Fe^{3+} - OH^- + HSO_5^- \rightarrow Fe^{2+} - .OOSO_3^- + H_2O$ $2Fe^{2+} - .OOSO_3^- + 2EGCG^+ \rightarrow 2Fe^{2+} \cdots EGCG + O_2 + 2SO_4^- + 2H^+$	[42]
	Glutathione(GSH)		-COOH -NH$_2$ -SH	$Fe^{2+} + H_2O_2 \rightarrow Fe^{3+} + OH \cdot + OH^-$	[85]
Polymer	Carboxymethyl cellulose(CMC)		-COOH	$Fe^0 + O_2 + 2H^+ \rightarrow Fe^{2+} + H_2O_2$ $2Fe^0 + 2H_2O \rightarrow 2Fe^{2+} + 2OH^- + H_2$ $Fe^{2+} + H_2O_2 \rightarrow Fe^{3+} + OH \cdot + OH^-$	[22]
	Chitosan(CS)		-COOH -NH$_2$ -OH	$Fe^{3+} + H_2O_2 \rightarrow Fe^{2+} + HOO \cdot + H^+$ $HOO \cdot + Fe^{2+} + H^+ \rightarrow Fe^{3+} + H_2O_2$ $Fe^{2+} + H_2O_2 \rightarrow Fe^{3+} + OH \cdot + OH^-$	[87]

4.2.2. Fe-Si Bonding with SiO_2 as Porous Supporting Materials for Iron-Based Materials to Increase Fe^{2+}

SiO_2 is a typical porous media material with stability and can be used as a supporting material for iron-based materials modification [3,88,89]. The unique silicon framework structure can form stable iron–silicon bonds with iron ions, which further promotes the catalytic performance of iron-based materials in AOPs. Ferroudj et al. used SiO_2 as support for magnetic nanoparticles to achieve good catalytic performance in a heterogeneous H_2O_2 system [88]. The particle size of Fe dispersed in the inner cavity of the silicon skeleton was small and firmly combined with silicon skeleton due to the stability of the silicon skeleton, which significantly improved the efficiency in removing pollutants [3,90]. Additionally, the existence of silica promoted the cycle of Fe^{3+}/Fe^{2+} in the iron-based composite material and promoted the content of effective Fe^{2+} [19]. Shukla et al. reported that SiO_2 could promote the redox of Fe^{3+}/Fe^{2+} by enhancing the stable combination between iron and silicon, although SiO_2 did not participate in the oxidation reaction [19]. The $OH^.$ and $HO_2^.$ produced during the redox process were the prominent radicals that degrade target pollutants (Equations (26) and (27)).

$$SiO_2-Fe^{3+}+H_2O_2 \rightarrow SiO_2-Fe^{3+}-H_2O_{2.} \rightarrow SiO_2-Fe^{2+}+HO_2^.+H^+ \tag{26}$$

$$SiO_2-Fe^{2+}+H_2O_2 \rightarrow SiO_2-Fe^{3+}+2OH^. \tag{27}$$
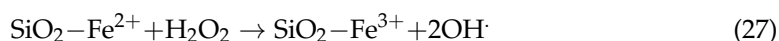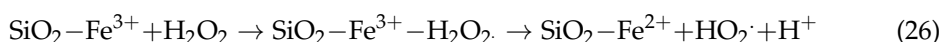
5. Key Properties and Commercialization Challenges of Iron-Based Materials in AOPs

5.1. Key Properties of Iron-Based Materials in AOPs

Modified iron-based materials have a variety of morphologies, including spherical, rod-like structure, core-shell structure, rock-like morphology, elongated hexagonal structure, the tubular and cambiform structure, etc. (Table 3). The critical properties of the modified iron-based materials showed that they obtained a larger BET surface area and a smaller lattice size, which further alleviated the agglomeration of the iron-based materials (Table 3) [86]. Meanwhile, the larger BET surface area and smaller lattice size could provide more catalytically active sites, enhancing the catalytic performance of composite iron-based materials in AOPs [41,64]. Moreover, stability is a crucial characteristic of heterogeneous catalysts in AOPs [86,88]. The composite materials achieved over 80% of the cycling degradations after the recycling used in AOPs (Table 3).

Table 3. Characteristics of iron-based materials in AOPs.
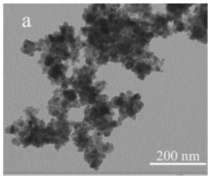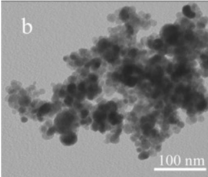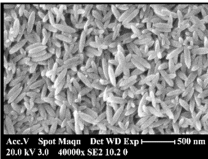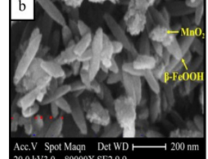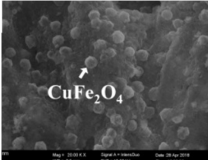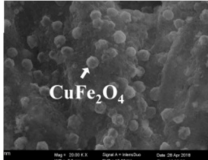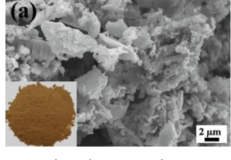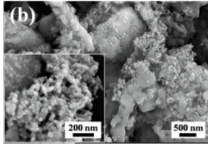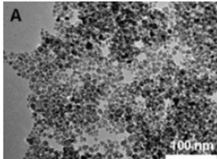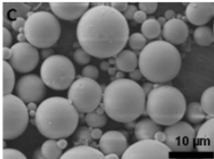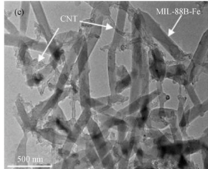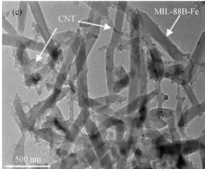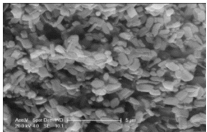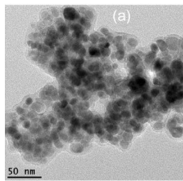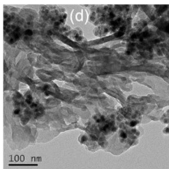
| Composite Material | Initial Iron-Based Materials | | | Modified Composite Iron-Based Materials | | | Stability of Composite Materials | | Reference |
| | Morphology | Properties | | Morphology | Properties | | Number of Cycles of Composite Materials | Degradation Efficiency at the Last Cycle | |
		BET Surface Area (m^2 g^{-1})	Lattice Size (nm)		BET Surface Area (m^2 g^{-1})	Lattice Size (nm)			
Fe$_3$O$_4$@β-CD	spherical	/	/	quasi-spherical	/	10–20	3	90%	[86]
β-FeOOH@MnO$_2$	nanorod structure	144.29	0.191	spindle-like-nanorod	341.58	0.133	5	90%	[64]
CuFe$_2$O$_4$/SEP	spherical	28.329	9.098	rough and densely porous	42.141	10.043	5	80.8%	[41]
Fe^0/Fe$_3$C	irregular shape with porous structure	/	/	nano-sphere, core/shell-like structure	/	20–30	3	92%	[91]

Table 3. *Cont.*

Composite Material	Initial Iron-Based Materials			Modified Composite Iron-Based Materials			Stability of Composite Materials		Reference
	Morphology	Properties		Morphology	Properties		Number of Cycles of Composite Materials	Degradation Efficiency at the Last Cycle	
		BET Surface Area $(m^2\ g^{-1})$	Lattice Size (nm)		BET Surface Area $(m^2\ g^{-1})$	Lattice Size (nm)			
γ-Fe_2O_3/SiO_2 MS	rock-like morphology	/	8.9	spherical shape	/	0.002	5	88%	[88]
MIL-88B-Fe/CNT	the cambiform architecture	54.82	/	the tubular and cambiform structure	98.43	/	3	100%	[39]
FeO/SiO_2	/	/	/	elongated hexagonal structure	/	0.00085–0.0015	3	98%	[19]
Fe_3O_4@C/gC_3N_4	spherical	13.67	/	spherical mesoporous structure	29.64	/	4	85%	[49]

Iron-based materials have the characteristics of environmental friendliness [92], variety of morphologies, recyclability, and potential in photocatalysis, which enable iron-based materials to prioritize in AOPs compared with the other commercial products [26,39,91]. First of all, iron-based materials are more available to be obtained in the environment [92]. Secondly, the various morphologies give iron-based materials a higher catalytic efficiency over other materials [19,39]. Thirdly, it can be easily removed from water by a simple magnetic separation method and reused [88,91,93]. Finally, it can extend the photocatalytic ability of TiO$_2$, which is widely used in wastewater treatment, from UV light irradiation to the visible light region [94,95]. Meanwhile, iron-based materials also have great photocatalytic potential in AOPs [26]. Therefore, heterogeneous AOPs based on iron-based materials enable wide-ranging commercialization in wastewater treatment [12,96]. However, the current research is mainly on a laboratory scale. Due to the lack of relevant research in practical AOPs-based wastewater treatment, iron-based materials still have some challenges in the commercial application of AOPs.

5.2. Commercialization Challenges of Iron-Based Materials in AOPs

Firstly, in the current experimental research, iron-based materials need to consume many solvents during the production process, which is not environmentally friendly [97,98]. Meanwhile, high pyrolysis temperature increases energy consumption during material preparation [46]. Therefore, developing a more environmentally friendly and simple preparation method for iron-based composites is still a challenge in the commercial application of iron-based materials in AOPs.

Secondly, the research in the laboratory is mainly to evaluate the cost-effectiveness of iron-based materials by evaluating the catalytic activity and reusability in AOPs [15]. The higher catalytic activity and longer reusability obtained in the laboratory may indicate the lower operating costs in AOPs [12,15]. Meanwhile, related experimental studies have confirmed that iron-based materials could generate H$_2$O$_2$ in situ in Fenton-based or electro-Fenton-based AOPs, reducing the dosing of oxidants [26,99], which may further reduce the operating cost of iron-based materials in the Fenton- or electro-Fenton-based AOPs. However, more pilot-scale experiments on the iron-based materials in natural industrial wastewater should be conducted, which benefits the more comprehensively evaluate the operating cost of materials in the commercial application in AOPs [96].

The management of these materials in the laboratory focuses on separating and recycling from water [15,49]. The materials are generally separated from water by filtration, centrifugation, magnetic sedimentation, etc., and further recycled [88,91]. The laboratory results indicated that the magnetic recycling method was the most effective way to reuse these materials [92]. However, there is still a lack of relevant data on the recycling effect of magnetic separation technology in actual wastewater treatment. Therefore, developing an efficient separation and recovery technology in practical wastewater treatment is also a challenge that limits the commercial application of iron-based materials in AOPs.

Modified iron-based composites have the advantages of cost-effectiveness, environmental friendliness, morphological diversity, high catalytic activity, and easy recycling and reuse. However, developing a green and simple preparation method for iron-based materials is still a challenge in current research. In the future, we should pay more attention to developing environmentally friendly preparation methods and more efficient separation methods of iron-based materials and produce more cost-effective composite materials for commercial applications in practical wastewater treatment.

6. Conclusions

The modification of iron-based materials significantly elevates the catalytic ability of iron-based materials in AOPs. The modified materials promote the catalytic potential of iron-based materials in AOPs through various mechanisms. Firstly, the electron-rich functional groups of the modified materials play an essential role in the electron transfer and the recombination of iron ions. Secondly, the bimetallic system, the FeS layer formed

by sulfide modification, the unique quinone structure of organic matter, and the hybrid carbon-based support materials have excellent electron transfer performance. Finally, environmentally friendly chelating agents, biopolymers, and porous support materials of SiO_2 have significant advantages in forming iron chelates or iron complexes.

Using environmentally friendly materials to modify iron-based materials can further increase iron-based materials' environmentally friendly potential and sustainability. Further evaluations include improving the cost and enhancing the health risks of modified iron-based materials in environment. In the dual carbon background, developing low-cost and high-efficiency iron-based composites for the degradation of refractory organic pollutants in AOPs is still worth exploring. Thus, using the relative advantages of different modified materials to develop iron-based materials with composite modification methods may be an excellent choice to improve the application of iron-based materials in the environment.

To promote the commercial application of iron-based materials in AOPs, we need to pay attention to the following issues: (1) it is necessary to conduct the further research on the green, environmentally friendly and simple preparation technologies of iron-based materials and exploit more cost-effective recycling processes of these materials; (2) the more cost-effective iron-based catalysts and iron-based composites should be further researched and performed in practical wastewater treatment; (3) photochemical AOPs are considered to be a clean, relatively cheap, simple, and generally more efficient process than chemical AOPs, therefore, the development of iron-based materials in photo-based AOPs is also an option for future commercial application of iron-based materials.

Supplementary Materials: The following supporting information can be downloaded at: https://www.mdpi.com/article/10.3390/w14091498/s1, Figure S1: The classification (percentage) of published papers based on organic pollutants, oxidation types, and iron-based materials; Table S1: Search strategy of keywords is based on the Web of Science; Classification of published papers based on searches of the Web of Science databases. Table S2: The functional modification type of iron-based materials is based on the literature classification; Supplementary Excel File S1: The detailed data of organic pollutants, oxidation types, iron-based materials, and modification types based on literature collected by Web of Science.

Author Contributions: Conceptualization, M.L., Z.Z. and C.H.; methodology, M.L., Z.Z. and D.W.; software, M.L., Z.Z. and J.L.; validation, X.C., X.L. and D.W.; formal analysis, M.L., Z.Z. and J.L.; writing—original draft preparation, M.L. and Z.Z.; writing—review and editing, Z.Z., D.W., X.C., X.L., C.H. and F.W.; supervision, C.H., Z.Z. and D.W.; project administration, C.H., D.W. and Z.Z.; funding acquisition, C.H. and Z.Z. All authors have read and agreed to the published version of the manuscript.

Funding: This work was supported by Shanghai Agriculture Applied Technology Development Program, China (Grant No.T20220206), Science and Technology Commission of Shanghai Municipality (19DZ1205202), National Natural Science Foundation of China (41971055, 41907270) and China Postdoctoral Science Foundation (grant number 2020M671069).

Institutional Review Board Statement: Not applicable.

Informed Consent Statement: Not application.

Data Availability Statement: Not application.

Acknowledgments: The authors wish to express the sincere gratitude to the reviewers for their time and effort.

Conflicts of Interest: The authors declare no conflict of interest.

References

1. Xu, J.; Zhang, X.; Sun, C.; Wan, J.; He, H.; Wang, F.; Dai, Y.; Yang, S.; Lin, Y.; Zhan, X. Insights into removal of tetracycline by persulfate activation with peanut shell biochar coupled with amorphous Cu-doped FeOOH composite in aqueous solution. *Environ. Sci. Pollut. Res.* **2019**, *26*, 2820–2834. [CrossRef] [PubMed]
2. Rayaroth, M.P.; Prasanthkumar, K.P.; Kang, Y.-G.; Lee, C.-S.; Chang, Y.-S. Degradation of carbamazepine by singlet oxygen from sulfidized nanoscale zero-valent iron-citric acid system. *Chem. Eng. J.* **2020**, *382*, 122828. [CrossRef]

3. Zhu, S.; Xu, Y.; Zhu, Z.; Liu, Z.; Wang, W. Activation of peroxymonosulfate by magnetic Co-Fe/SiO$_2$ layered catalyst derived from iron sludge for ciprofloxacin degradation. *Chem. Eng. J.* **2020**, *384*, 123298. [CrossRef]

4. Amina; Si, X.; Wu, K.; Si, Y.; Yousaf, B. Mechanistic insights into the reactive radicals-assisted degradation of sulfamethoxazole via calcium peroxide activation by manganese-incorporated iron oxide-graphene nanocomposite: Formation of radicals and degradation pathway. *Chem. Eng. J.* **2020**, *384*, 123360. [CrossRef]

5. Ghanbari, F.; Moradi, M. Application of peroxymonosulfate and its activation methods for degradation of environmental organic pollutants: Review. *Chem. Eng. J.* **2017**, *310*, 41–62. [CrossRef]

6. Liu, C.; Liu, S.; Liu, L.; Tian, X.; Liu, L.; Xia, Y.; Liang, X.; Wang, Y.; Song, Z.; Zhang, Y.; et al. Novel carbon based Fe-Co oxides derived from Prussian blue analogues activating peroxymonosulfate: Refractory drugs degradation without metal leaching. *Chem. Eng. J.* **2020**, *379*, 122274. [CrossRef]

7. Heidarpour, H.; Padervand, M.; Soltanieh, M.; Vossoughi, M. Enhanced decolorization of rhodamine B solution through simultaneous photocatalysis and persulfate activation over Fe/C$_3$N$_4$ photocatalyst. *Chem. Eng. Res. Des.* **2020**, *153*, 709–720. [CrossRef]

8. Su, S.; Liu, Y.; He, W.; Tang, X.; Jin, W.; Zhao, Y. A novel graphene oxide-carbon nanotubes anchored alpha-FeOOH hybrid activated persulfate system for enhanced degradation of Orange II. *J. Environ. Sci.* **2019**, *83*, 73–84. [CrossRef]

9. Poyatos, J.M.; Muñío, M.M.; Almecija, M.C.; Torres, J.C.; Hontoria, E.; Osorio, F. Advanced Oxidation Processes for Wastewater Treatment: State of the Art. *Water Air Soil Pollut.* **2009**, *205*, 187–204. [CrossRef]

10. Lee, J.; von Gunten, U.; Kim, J.H. Persulfate-Based Advanced Oxidation: Critical Assessment of Opportunities and Roadblocks. *Environ. Sci. Technol.* **2020**, *54*, 3064–3081. [CrossRef]

11. Li, X.; Wu, D.; Hua, T.; Lan, X.; Han, S.; Cheng, J.; Du, K.S.; Hu, Y.; Chen, Y. Micro/macrostructure and multicomponent design of catalysts by MOF-derived strategy: Opportunities for the application of nanomaterials-based advanced oxidation processes in wastewater treatment. *Sci. Total Environ.* **2022**, *804*, 150096. [CrossRef] [PubMed]

12. Cardoso, I.M.F.; Cardoso, R.M.F.; da Silva, J. Advanced Oxidation Processes Coupled with Nanomaterials for Water Treatment. *Nanomaterials* **2021**, *11*, 2045. [CrossRef] [PubMed]

13. Bethi, B.; Sonawane, S.H.; Bhanvase, B.A.; Gumfekar, S.P. Nanomaterials-based advanced oxidation processes for wastewater treatment: A review. *Chem. Eng. Process.-Process Intensif.* **2016**, *109*, 178–189. [CrossRef]

14. Xiao, R.; Luo, Z.; Wei, Z.; Luo, S.; Spinney, R.; Yang, W.; Dionysiou, D.D. Activation of peroxymonosulfate/persulfate by nanomaterials for sulfate radical-based advanced oxidation technologies. *Curr. Opin. Chem. Eng.* **2018**, *19*, 51–58. [CrossRef]

15. Heidari, Z.; Pelalak, R.; Alizadeh, R.; Oturan, N.; Shirazian, S.; Oturan, M.A. Application of Mineral Iron-Based Natural Catalysts in Electro-Fenton Process: A Comparative Study. *Catalysts* **2021**, *11*, 57. [CrossRef]

16. Wang, J.; Wang, S. Activation of persulfate (PS) and peroxymonosulfate (PMS) and application for the degradation of emerging contaminants. *Chem. Eng. J.* **2018**, *334*, 1502–1517. [CrossRef]

17. Qu, J.; Che, T.; Shi, L.; Lu, Q.; Qi, S. A novel magnetic silica supported spinel ferrites NiFe2O4 catalyst for heterogeneous Fenton-like oxidation of rhodamine B. *Chin. Chem. Lett.* **2019**, *30*, 1198–1203. [CrossRef]

18. Lee, H.; Yoo, H.-Y.; Choi, J.; Nam, I.-H.; Lee, S.; Lee, S.; Kim, J.-H.; Lee, C.; Lee, J. Oxidizing Capacity of Periodate Activated with Iron-Based Bimetallic Nanoparticles. *Environ. Sci. Technol.* **2014**, *48*, 8086–8093. [CrossRef]

19. Shukla, P.; Wang, S.; Sun, H.; Ang, H.-M.; Tade, M. Adsorption and heterogeneous advanced oxidation of phenolic contaminants using Fe loaded mesoporous SBA-15 and H$_2$O$_2$. *Chem. Eng. J.* **2010**, *164*, 255–260. [CrossRef]

20. Cheng, M.; Zeng, G.; Huang, D.; Lai, C.; Liu, Y.; Xu, P.; Zhang, C.; Wan, J.; Hu, L.; Xiong, W.; et al. Salicylic acid-methanol modified steel converter slag as heterogeneous Fenton-like catalyst for enhanced degradation of alachlor. *Chem. Eng. J.* **2017**, *327*, 686–693. [CrossRef]

21. Yao, S.H.; Chen, X.J.; Gomez, M.A.; Ma, X.C.; Wang, H.B.; Zang, S.Y. One-step synthesis of zerovalent-iron-biochar composites to activate persulfate for phenol degradation. *Water Sci. Technol.* **2019**, *80*, 1851–1860. [CrossRef] [PubMed]

22. Silva, L.L.S.; Caldara, J.A.; Rocco, A.M.; Borges, C.P.; Fonseca, F.V. Evaluation of Nano Zero-Valent Iron (nZVI) Activity in Solution and Immobilized in Hydrophilic PVDF Membrane for Drimaren Red X-6BN and Bisphenol-a Removal in Water. *Processes* **2019**, *7*, 904. [CrossRef]

23. Nguyen, V.-T.; Hung, C.-M.; Nguyen, T.-B.; Chang, J.-H.; Wang, T.-H.; Wu, C.-H.; Lin, Y.-L.; Chen, C.-W.; Dong, C.-D. Efficient Heterogeneous Activation of Persulfate by Iron-Modified Biochar for Removal of Antibiotic from Aqueous Solution: A Case Study of Tetracycline Removal. *Catalysts* **2019**, *9*, 49. [CrossRef]

24. Kajani, A.A.; Bordbar, A.-K. Biogenic magnetite nanoparticles: A potent and environmentally benign agent for efficient removal of azo dyes and phenolic contaminants from water. *J. Hazard. Mater.* **2019**, *366*, 268–274. [CrossRef]

25. Zhang, X.; Chen, Y.; Zhao, N.; Liu, H.; Wei, Y. Citrate modified ferrihydrite microstructures: Facile synthesis, strong adsorption and excellent Fenton-like catalytic properties. *RSC Adv.* **2014**, *4*, 21575–21583. [CrossRef]

26. Luo, H.; Zeng, Y.; He, D.; Pan, X. Application of iron-based materials in heterogeneous advanced oxidation processes for wastewater treatment: A review. *Chem. Eng. J.* **2021**, *407*, 127191. [CrossRef]

27. Dong, C.-D.; Chen, C.-W.; Tsai, M.-L.; Chang, J.-H.; Lyu, S.-Y.; Hung, C.-M. Degradation of 4-nonylphenol in marine sediments by persulfate over magnetically modified biochars. *Bioresour. Technol.* **2019**, *281*, 143–148. [CrossRef]

28. Zhao, G.; Zou, J.; Chen, X.; Liu, L.; Wang, Y.; Zhou, S.; Long, X.; Yu, J.; Jiao, F. Iron-based catalysts for persulfate-based advanced oxidation process: Microstructure, property and tailoring. *Chem. Eng. J.* **2021**, *421*, 127845. [CrossRef]

29. Malakootian, M.; Shahesmaeili, A.; Faraji, M.; Amiri, H.; Silva Martinez, S. Advanced oxidation processes for the removal of organophosphorus pesticides in aqueous matrices: A systematic review and meta-analysis. *Process Saf. Environ. Prot.* **2020**, *134*, 292–307. [CrossRef]

30. Azari, A.; Nabizadeh, R.; Nasseri, S.; Mahvi, A.H.; Mesdaghinia, A.R. Comprehensive systematic review and meta-analysis of dyes adsorption by carbon-based adsorbent materials: Classification and analysis of last decade studies. *Chemosphere* **2020**, *250*, 126238. [CrossRef]

31. Zhang, S.; Gao, H.; Huang, Y.; Wang, X.; Hayat, T.; Li, J.; Xu, X.; Wang, X. Ultrathin g-C3N4 nanosheets coupled with amorphous Cu-doped FeOOH nanoclusters as 2D/0D heterogeneous catalysts for water remediation. *Environ. Sci.-Nano* **2018**, *5*, 1179–1190. [CrossRef]

32. Wang, J.; Shen, M.; Gong, Q.; Wang, X.; Cai, J.; Wang, S.; Chen, Z. One-step preparation of ZVI-sludge derived biochar without external source of iron and its application on persulfate activation. *Sci. Total Environ.* **2020**, *714*, 136728. [CrossRef] [PubMed]

33. Li, X.; Guo, W.; Liu, Z.; Wang, R.; Liu, H. Quinone-modified NH2-MIL-101(Fe) composite as a redox mediator for improved degradation of bisphenol A. *J. Hazard. Mater.* **2017**, *324*, 665–672. [CrossRef] [PubMed]

34. Li, Z.; Sun, Y.; Yang, Y.; Han, Y.; Wang, T.; Chen, J.; Tsang, D.C.W. Biochar-supported nanoscale zero-valent iron as an efficient catalyst for organic degradation in groundwater. *J. Hazard. Mater.* **2020**, *383*, 121240. [CrossRef] [PubMed]

35. Belattar, S.; Debbache, N.; Ghoul, I.; Sehili, T.; Abdessemed, A. Photodegradation of phenol red in the presence of oxyhydroxide of Fe(III) (Goethite) under artificial and a natural light. *Water Environ. J.* **2018**, *32*, 358–365. [CrossRef]

36. Salari, H. Kinetics and mechanism of enhanced photocatalytic activity under visible light irradiation using Cr2O3/Fe2O3 nanostructure derived from bimetallic metal organic framework. *J. Environ. Chem. Eng.* **2019**, *7*, 103092. [CrossRef]

37. Wu, Y.Y.; Yang, C.X.; Yan, X.P. Fabrication of metal-organic framework MIL-88B films on stainless steel fibers for solid-phase microextraction of polychlorinated biphenyls. *J. Chromatogr. A* **2014**, *1334*, 1–8. [CrossRef]

38. Li, X.; Guo, W.; Liu, Z.; Wang, R.; Liu, H. Fe-based MOFs for efficient adsorption and degradation of acid orange 7 in aqueous solution via persulfate activation. *Appl. Surf. Sci.* **2016**, *369*, 130–136. [CrossRef]

39. Zhang, H.; Chen, S.; Zhang, H.; Fan, X.; Gao, C.; Yu, H.; Quan, X. Carbon nanotubes-incorporated MIL-88B-Fe as highly efficient Fenton-like catalyst for degradation of organic pollutants. *Front. Environ. Sci. Eng.* **2019**, *13*, 18. [CrossRef]

40. Taleb, M.F.A. Adsorption and photocatalytic degradation of 2-CP in wastewater onto CS/CoFe2O4 nanocomposite synthesized using gamma radiation. *Carbohydr. Polym.* **2014**, *114*, 65–72. [CrossRef]

41. Liu, D.; Wang, C.; Song, Y.; Wei, Y.; He, L.; Lan, B.; He, X.; Wang, J. Effective mineralization of quinoline and bio-treated coking wastewater by catalytic ozonation using CuFe2O4/Sepiolite catalyst: Efficiency and mechanism. *Chemosphere* **2019**, *227*, 647–656. [CrossRef]

42. Tan, C.; Jian, X.; Dong, Y.; Lu, X.; Liu, X.; Xiang, H.; Cui, X.; Deng, J.; Gao, H. Activation of peroxymonosulfate by a novel EGCE@Fe3O4 nanocomposite: Free radical reactions and implication for the degradation of sulfadiazine. *Chem. Eng. J.* **2019**, *359*, 594–603. [CrossRef]

43. Chen, L.; Zuo, X.; Yang, S.; Cai, T.; Ding, D. Rational design and synthesis of hollow Co3O4@Fe2O3 core-shell nanostructure for the catalytic degradation of norfloxacin by coupling with peroxymonosulfate. *Chem. Eng. J.* **2019**, *359*, 373–384. [CrossRef]

44. Yue, S.; Qiyan, F.; Xiangdong, L. Application of response surface methodology to optimize degradation of polyacrylamide in aqueous solution using heterogeneous Fenton process. *Desalination Water Treat.* **2013**, *53*, 1923–1932. [CrossRef]

45. Peng, Q.; Ding, Y.; Zhu, L.; Zhang, G.; Tang, H. Fast and complete degradation of norfloxacin by using Fe/Fe3C@NG as a bifunctional catalyst for activating peroxymonosulfate. *Sep. Purif. Technol.* **2018**, *202*, 307–317. [CrossRef]

46. Dai, X.-H.; Fan, H.-X.; Yi, C.-Y.; Dong, B.; Yuan, S.-J. Solvent-free synthesis of a 2D biochar stabilized nanoscale zerovalent iron composite for the oxidative degradation of organic pollutants. *J. Mater. Chem. A* **2019**, *7*, 6849–6858. [CrossRef]

47. Boruah, P.K.; Sharma, B.; Karbhal, I.; Shelke, M.V.; Das, M.R. Ammonia-modified graphene sheets decorated with magnetic Fe3O4 nanoparticles for the photocatalytic and photo-Fenton degradation of phenolic compounds under sunlight irradiation. *J. Hazard. Mater.* **2017**, *325*, 90–100. [CrossRef]

48. Liu, L.; Xu, X.; Li, Y.; Su, R.; Li, Q.; Zhou, W.; Gao, B.; Yue, Q. One-step synthesis of "nuclear-shell" structure iron-carbon nanocomposite as a persulfate activator for bisphenol A degradation. *Chem. Eng. J.* **2020**, *382*, 122780. [CrossRef]

49. Guo, F.; Lu, J.; Liu, Q.; Zhang, P.; Zhang, A.; Cai, Y.; Wang, Q. Degradation of Acid Orange 7 by peroxymonosulfate activated with the recyclable nanocomposites of g-C3N4 modified magnetic carbon. *Chemosphere* **2018**, *205*, 297–307. [CrossRef]

50. Luo, H.; Lin, Q.; Zhang, X.; Huang, Z.; Liu, S.; Jiang, J.; Xiao, R.; Liao, X. New insights into the formation and transformation of active species in nZVI/BC activated persulfate in alkaline solutions. *Chem. Eng. J.* **2019**, *359*, 1215–1223. [CrossRef]

51. Daud, N.K.; Ahmad, M.A.; Hameed, B.H. Decolorization of Acid Red 1 dye solution by Fenton-like process using Fe-Montmorillonite K10 catalyst. *Chem. Eng. J.* **2010**, *165*, 111–116. [CrossRef]

52. Danish, M.; Gu, X.; Lu, S.; Xu, M.; Zhang, X.; Fu, X.; Xue, Y.; Miao, Z.; Naqvi, M.; Nasir, M. Role of reactive oxygen species and effect of solution matrix in trichloroethylene degradation from aqueous solution by zeolite-supported nano iron as percarbonate activator. *Res. Chem. Intermed.* **2016**, *42*, 6959–6973. [CrossRef]

53. Zhao, X.; Zhu, L.; Zhang, Y.; Yan, J.; Lu, X.; Huang, Y.; Tang, H. Removing organic contaminants with bifunctional iron modified rectorite as efficient adsorbent and visible light photo-Fenton catalyst. *J. Hazard. Mater.* **2012**, *215*, 57–64. [CrossRef] [PubMed]

54. Niu, H.; He, D.; Yang, Y.; Lv, H.; Cai, Y.; Liang, Y. Long-lasting activity of Fe-0-C internal microelectrolysis-Fenton system assisted by Fe@C-montmorillonites nanocomposites. *Appl. Catal. B-Environ.* **2019**, *256*, 117820. [CrossRef]

55. Lu, H.; Sui, M.; Yuan, B.; Wang, J.; Lv, Y. Efficient degradation of nitrobenzene by Cu-Co-Fe-LDH catalyzed peroxymonosulfate to produce hydroxyl radicals. *Chem. Eng. J.* **2019**, *357*, 140–149. [CrossRef]

56. Ji, Q.; Li, J.; Xiong, Z.; Lai, B. Enhanced reactivity of microscale Fe/Cu bimetallic particles (mFe/Cu) with persulfate (PS) for p-nitrophenol (PNP) removal in aqueous solution. *Chemosphere* **2017**, *172*, 10–20. [CrossRef]

57. Li, Y.; Li, X.; Han, D.; Huang, W.; Yang, C. New insights into the role of Ni loading on the surface structure and the reactivity of nZVI toward tetrabromo- and tetrachlorobisphenol A. *Chem. Eng. J.* **2017**, *311*, 173–182. [CrossRef]

58. Gomez-Obando, V.A.; Garcia-Mora, A.M.; Basante, J.S.; Hidalgo, A.; Galeano, L.A. CWPO Degradation of Methyl Orange at Circumneutral pH: Multi-Response Statistical Optimization, Main Intermediates and by-Products. *Front. Chem.* **2019**, *7*, 772. [CrossRef]

59. Silveira, J.E.; Barreto-Rodrigues, M.; Cardoso, T.O.; Pliego, G.; Munoz, M.; Zazo, J.A.; Casas, J.A. Nanoscale Fe/Ag particles activated persulfate: Optimization using response surface methodology. *Water Sci. Technol.* **2017**, *75*, 2216–2224. [CrossRef]

60. Liu, X.; Fan, J.-H.; Ma, L.-M. Elimination of 4-chlorophenol in aqueous solution by the bimetallic Al-Fe/O-2 at normal temperature and pressure. *Chem. Eng. J.* **2014**, *236*, 274–284. [CrossRef]

61. Yamaguchi, R.; Kurosu, S.; Suzuki, M.; Kawase, Y. Hydroxyl radical generation by zero-valent iron/Cu (ZVI/Cu) bimetallic catalyst in wastewater treatment: Heterogeneous Fenton/Fenton-like reactions by Fenton reagents formed in-situ under oxic conditions. *Chem. Eng. J.* **2018**, *334*, 1537–1549. [CrossRef]

62. Song, S.; Su, M.; Adeleye, A.S.; Zhang, Y.; Zhou, X. Optimal design and characterization of sulfide-modified nanoscale zerovalent iron for diclofenac removal. *Appl. Catal. B-Environ.* **2017**, *201*, 211–220. [CrossRef]

63. Huang, R.; Liu, Y.; Chen, Z.; Pan, D.; Li, Z.; Wu, M.; Shek, C.-H.; Wu, C.M.L.; Lai, J.K.L. Fe-Species-Loaded Mesoporous MnO2 Superstructural Requirements for Enhanced Catalysis. *Acs Appl. Mater. Interfaces* **2015**, *7*, 3949–3959. [CrossRef] [PubMed]

64. Lyu, C.; He, D.; Mou, Z.; Yang, X. Synergetic activation of peroxymonosulfate by MnO2-loaded beta-FeOOH catalyst for enhanced degradation of organic pollutant in water. *Sci. Total Environ.* **2019**, *693*, 133589. [CrossRef]

65. Wei, X.; Yin, H.; Peng, H.; Chen, R.; Lu, G.; Dang, Z. Reductive debromination of decabromodiphenyl ether by iron sulfide-coated nanoscale zerovalent iron: Mechanistic insights from Fe(II) dissolution and solvent kinetic isotope effects. *Environ. Pollut.* **2019**, *253*, 161–170. [CrossRef]

66. Li, J.; Zhang, X.; Sun, Y.; Liang, L.; Pan, B.; Zhang, W.; Guan, X. Advances in Sulfidation of Zerovalent Iron for Water Decontamination. *Environ. Sci. Technol.* **2017**, *51*, 13533–13544. [CrossRef]

67. Dong, H.; Zhang, C.; Deng, J.; Jiang, Z.; Zhang, L.; Cheng, Y.; Hou, K.; Tang, L.; Zeng, G. Factors influencing degradation of trichloroethylene by sulfide-modified nanoscale zero-valent iron in aqueous solution. *Water Res* **2018**, *135*, 1–10. [CrossRef]

68. Tang, J.; Tang, L.; Feng, H.; Zeng, G.; Dong, H.; Zhang, C.; Huang, B.; Deng, Y.; Wang, J.; Zhou, Y. pH-dependent degradation of p-nitrophenol by sulfidated nanoscale zerovalent iron under aerobic or anoxic conditions. *J. Hazard. Mater.* **2016**, *320*, 581–590. [CrossRef]

69. Dong, H.; Hou, K.; Qiao, W.; Cheng, Y.; Zhang, L.; Wang, B.; Li, L.; Wang, Y.; Ning, Q.; Zeng, G. Insights into enhanced removal of TCE utilizing sulfide-modified nanoscale zero-valent iron activated persulfate. *Chem. Eng. J.* **2019**, *359*, 1046–1055. [CrossRef]

70. Fan, D.; Lan, Y.; Tratnyek, P.G.; Johnson, R.L.; Filip, J.; O'Carroll, D.M.; Nunez Garcia, A.; Agrawal, A. Sulfidation of Iron-Based Materials: A Review of Processes and Implications for Water Treatment and Remediation. *Environ. Sci. Technol.* **2017**, *51*, 13070–13085. [CrossRef]

71. Wang, Y.; Zhu, X.; Feng, D.; Hodge, A.K.; Hu, L.; Lu, J.; Li, J. Biochar-Supported FeS/Fe3O4 Composite for Catalyzed Fenton-Type Degradation of Ciprofloxacin. *Catalysts* **2019**, *9*, 1062. [CrossRef]

72. Pang, Y.; Luo, K.; Tang, L.; Li, X.; Song, Y.; Li, C.Y.; Wang, L.P. Preparation and application of magnetic nitrogen-doped rGO for persulfate activation. *Environ. Sci. Pollut. Res. Int.* **2018**, *25*, 30575–30584. [CrossRef]

73. Bin, Q.; Lin, B.; Zhu, K.; Shen, Y.; Man, Y.; Wang, B.; Lai, C.; Chen, W. Superior trichloroethylene removal from water by sulfide-modified nanoscale zero-valent iron/graphene aerogel composite. *J. Environ. Sci.* **2020**, *88*, 90–102. [CrossRef] [PubMed]

74. Huang, X.; Niv, Y.; Hu, W. Fe/Fe3C nanoparticles loaded on Fe/N-doped graphene as an efficient heterogeneous Fenton catalyst for degradation of organic pollutants. *Colloids Surf. A-Physicochem. Eng. Asp.* **2017**, *518*, 145–150. [CrossRef]

75. Wei, L.; Zhang, Y.; Chen, S.; Zhu, L.; Liu, X.; Kong, L.; Wang, L. Synthesis of nitrogen-doped carbon nanotubes-FePO4 composite from phosphate residue and its application as effective Fenton-like catalyst for dye degradation. *J. Environ. Sci.* **2019**, *76*, 188–198. [CrossRef] [PubMed]

76. Li, M.; Luo, R.; Wang, C.; Zhang, M.; Zhang, W.; Klu, P.K.; Yan, Y.; Qi, J.; Sun, X.; Wang, L.; et al. Iron-tannic modified cotton derived Fe-0/graphitized carbon with enhanced catalytic activity for bisphenol A degradation. *Chem. Eng. J.* **2019**, *372*, 774–784. [CrossRef]

77. Peng, G.; Zhang, M.; Deng, S.; Shan, D.; He, Q.; Yu, G. Adsorption and catalytic oxidation of pharmaceuticals by nitrogen-doped reduced graphene oxide/Fe3O4 nanocomposite. *Chem. Eng. J.* **2018**, *341*, 361–370. [CrossRef]

78. Zhao, Y.; Yang, L.; Chen, S.; Wang, X.; Ma, Y.; Wu, Q.; Jiang, Y.; Qian, W.; Hu, Z. Can boron and nitrogen co-doping improve oxygen reduction reaction activity of carbon nanotubes? *J. Am. Chem. Soc.* **2013**, *135*, 1201–1204. [CrossRef]

79. Chen, X.; Wang, L.; Sun, W.; Yang, Z.; Jin, J.; You, D.; Liu, G. Enhanced electrochemical advanced oxidation on boride activated carbon: The influences of boron groups. *Electrochim. Acta* **2021**, *400*, 139462. [CrossRef]

80. Huang, M.; Wang, X.; Liu, C.; Fang, G.; Gao, J.; Wang, Y.; Zhou, D. Facile ball milling preparation of sulfur-doped carbon as peroxymonosulfate activator for efficient removal of organic pollutants. *J. Environ. Chem. Eng.* **2021**, *9*, 106536. [CrossRef]

81. Pan, Y.; Zhou, M.; Cai, J.; Tian, Y.; Zhang, Y. Mechanism study of nitrilotriacetic acid-modified premagnetized Fe-0/H2O2 for removing sulfamethazine. *Chem. Eng. J.* **2019**, *374*, 1180–1190. [CrossRef]

82. Tan, C.; Lu, X.; Cui, X.; Jian, X.; Hu, Z.; Dong, Y.; Liu, X.; Huang, J.; Deng, L. Novel activation of peroxymonosulfate by an easily recyclable VC@Fe3O4 nanoparticles for enhanced degradation of sulfadiazine. *Chem. Eng. J.* **2019**, *363*, 318–328. [CrossRef]

83. Dong, Y.; Cui, X.; Lu, X.; Jian, X.; Xu, Q.; Tan, C. Enhanced degradation of sulfadiazine by novel beta-alaninediacetic acid-modified Fe3O4 nanocomposite coupled with peroxymonosulfate. *Sci. Total Environ.* **2019**, *662*, 490–500. [CrossRef] [PubMed]

84. Nadejde, C.; Neamtu, M.; Hodoroaba, V.D.; Schneider, R.J.; Paul, A.; Ababei, G.; Panne, U. Tannic acid- and natural organic matter-coated magnetite as green Fenton-like catalysts for the removal of water pollutants. *J. Nanopart. Res.* **2015**, *17*, 1–10. [CrossRef]

85. Zhou, R.; Shen, N.; Zhao, J.; Su, Y.; Ren, H. Glutathione-coated Fe3O4 nanoparticles with enhanced Fenton-like activity at neutral pH for degrading 2,4-dichlorophenol. *J. Mater. Chem. A* **2018**, *6*, 1275–1283. [CrossRef]

86. Wang, M.; Fang, G.; Liu, P.; Zhou, D.; Ma, C.; Zhang, D.; Zhan, J. Fe$_3$O$_4$ @β-CD nanocomposite as heterogeneous Fenton-like catalyst for enhanced degradation of 4-chlorophenol (4-CP). *Appl. Catal. B Environ.* **2016**, *188*, 113–122. [CrossRef]

87. Nadejde, C.; Neamtu, M.; Hodoroaba, V.D.; Schneider, R.J.; Ababei, G.; Panne, U. Hybrid iron-based core-shell magnetic catalysts for fast degradation of bisphenol A in aqueous systems. *Chem. Eng. J.* **2016**, *302*, 587–594. [CrossRef]

88. Ferroudj, N.; Nzimoto, J.; Davidson, A.; Talbot, D.; Briot, E.; Dupuis, V.; Bee, A.; Medjram, M.S.; Abramson, S. Maghemite nanoparticles and maghemite/silica nanocomposite microspheres as magnetic Fenton catalysts for the removal of water pollutants. *Appl. Catal. B-Environ.* **2013**, *136*, 9–18. [CrossRef]

89. Mandal, S.; Adhikari, S.; Pu, S.; Wang, X.; Kim, D.-H.; Patel, R.K. Interactive Fe$_2$O$_3$/porous SiO$_2$ nanospheres for photocatalytic degradation of organic pollutants: Kinetic and mechanistic approach. *Chemosphere* **2019**, *234*, 596–607. [CrossRef]

90. Rasoulifard, M.H.; Monfared, H.H.; Masoudian, S. Photo-assisted hetero-Fenton decolorization of azo dye from contaminated water by Fe-Si mixed oxide nanocomposite. *Environ. Technol.* **2011**, *32*, 1627–1635. [CrossRef]

91. Zhu, S.; Wang, W.; Xu, Y.; Zhu, Z.; Liu, Z.; Cui, F. Iron sludge-derived magnetic Fe-0/Fe3C catalyst for oxidation of ciprofloxacin via peroxymonosulfate activation. *Chem. Eng. J.* **2019**, *365*, 99–110. [CrossRef]

92. Ambashta, R.D.; Sillanpaa, M. Water purification using magnetic assistance: A review. *J. Hazard Mater.* **2010**, *180*, 38–49. [CrossRef] [PubMed]

93. Graham, L.J.; Atwater, J.E.; Jovanovic, G.N. Chlorophenol dehalogenation in a magnetically stabilized fluidized bed reactor. *AIChE J.* **2006**, *52*, 1083–1093. [CrossRef]

94. Ohno, T. Development of visible light sensitive TiO2 photocatalysts and their sensitization using Fe^{3+} ions. *J. Jpn. Pet. Inst.* **2006**, *49*, 168–176. [CrossRef]

95. Jian Zhu, J.R.; Huo, Y.; Bian, Z.; Li, H. Nanocrystalline Fe/TiO$_2$ Visible Photocatalyst with a Mesoporous Structure Prepared via a Nonhydrolytic Sol-Gel Route. *J. Phys. Chem. C* **2007**, *111*, 18965–18969.

96. Kurian, M. Advanced oxidation processes and nanomaterials—A review. *Clean. Eng. Technol.* **2021**, *2*, 100090. [CrossRef]

97. Kohantorabi, M.; Hosseinifard, M.; Kazemzadeh, A. Catalytic activity of a magnetic Fe$_2$O$_3$@CoFe$_2$O$_4$ nanocomposite in peroxymonosulfate activation for norfloxacin removal. *New J. Chem.* **2020**, *44*, 4185–4198. [CrossRef]

98. Jiang, Z.; Li, J.; Jiang, D.; Gao, Y.; Chen, Y.; Wang, W.; Cao, B.; Tao, Y.; Wang, L.; Zhang, Y. Removal of atrazine by biochar-supported zero-valent iron catalyzed persulfate oxidation: Reactivity, radical production and transformation pathway. *Environ. Res.* **2020**, *184*, 109260. [CrossRef]

99. Yu, J.; Hou, X.; Hu, X.; Yuan, H.; Wang, J.; Chen, C. Efficient degradation of chloramphenicol by zero-valent iron microspheres and new insights in mechanisms. *Appl. Catal. B Environ.* **2019**, *256*, 117876. [CrossRef]